Journal of Materials Science: Materials in Electronics (2019) 30:20770–20777
https://doi.org/10.1007/s10854-019-02444-0

Effect of minor scandium addition on the microstructure and properties of Al–50Si alloys for electronic packaging

Shuaishuai Yu[1] · Richu Wang[1,2,3] · Chaoqun Peng[1] · Zhiyong Cai[1,2] · Xiang Wu[1] · Yan Feng[1,2] · Xiaofeng Wang[1]

Received: 5 September 2019 / Accepted: 23 October 2019 / Published online: 4 November 2019

Abstract
Al–50Si alloys for electronic packaging were prepared by gas atomization following hot press sintering, and the influences of adding minor Sc (0.3%) on microstructure and mechanical and thermo-physical properties were studied. The Si phase exhibits a semi-continuous network structure with an average size of 15–20 μm in the alloys with and without Sc addition. Transmission electron microscopy observation indicates that a fine spherical Sc-rich particle distributes at the interface between the Al matrix and Si phase in the Al–50Si-Sc alloy, which is further identified as $AlSi_2Sc_2$ (V-phase). The tensile strength, flexural strength, and hardness of the Al–50Si alloy are improved by 16.2%, 8.9%, and 14.7%, respectively, with the introduction of Sc. However, the coefficient of thermal expansion and thermal conductivity decreases slightly in the Al–50Si–Sc alloy as compared with the Al–50Si alloy. The increased strength is mainly attributed to the formation of fine spherical $AlSi_2Sc_2$ phase which strengthens the Al matrix.

1 Introduction

The rapid growing of electronic information technology and the shortened update cycle leads to the development of high-power, miniaturization, complication, and high reliability in the related fields such as microwave circuits and electronic components. Therefore, the development of high-performance electronic packaging materials is particularly important for the electronics industry. Excellent electronic packaging materials need good mechanical properties while achieving low thermal expansion coefficient and high thermal conductivity [1].

Al–high Si alloys are also named Si phase-reinforced Al matrix composites (AMCs) [2, 3]. By controlling the content of Si, the Al–Si alloys show good properties, including low density, relatively high thermal conductivity, and low coefficient of thermal expansion (CTE) [4–6]. However, excessive coarse primary and eutectic Si phase are present in the Al–Si alloys prepared by traditional ingot metallurgy. The tip of the coarse Si phase is prone to stress concentration and tends to be the source of crack propagation, which deteriorates the properties of the alloys as well as workability, palatability, and laser weldability [7, 8]. Therefore, the microstructure of the Al–Si alloys with high Si content must be well optimized to improve the properties and solve the inconvenience of subsequent processing [9].

At present, various methods can be used to modify the distribution and morphology of the Si phase. The simplest and most effective route is the introduction of modifiers, such as P [10] and rare earth elements (Er, Nd, Ce et al.) [11–13]. However, Hogg and Atkinson [14] suggested that the addition of the modifier alone does not significantly improve the primary Si phase. Generally, Sc is widely used as an important alloying element in Al alloys, which can refine the grain and strengthen the matrix. Additionally, adding Sc element can improve the wettability during solidification and effectively improve the eutectic Si phase in the Al–Si alloy [15]. However, Kim et al. [16] studied the as-cast Al-20Si alloy with different contents of Sc and found that Sc has no obvious modification effect on primary Si. Moreover, when the Sc is introduced to Al–Si alloys, a stable $AlSi_2Sc_2$ intermetallic phase is formed instead of Al_3Sc [17].

On the other hand, rapid solidification technology can effectively improve the deficiency of adding modifiers,

✉ Zhiyong Cai
zycaimse@163.com

[1] School of Materials Science and Engineering, Central South University, Changsha 410083, China

[2] National Key Laboratory of Science and Technology for National Defence on High-Strength Structural Materials, Central South University, Changsha 410083, China

[3] Key Laboratory of Electronic Packaging and Advanced Functional Materials, Changsha 410083, Hunan, China

and the resulting morphology and size of primary Si is completely different from the as-cast state [4, 18]. Furthermore, rapid solidification technology also has the characteristics of uniform composition and low segregation, which are beneficial for obtaining good mechanical properties and some special physical properties. Although adding Sc to the as-cast Al–Si alloys has been fully explored, it has mainly focused on the as-cast hypoeutectic or eutectic Al–Si alloys. The effect of V-phase on the mechanical and thermo-physical properties of Al–high Si alloys is less reported, especially in combination with rapid solidification technology.

In the present work, Al–50Si and Al–50Si–0.3Sc alloys for electronic packaging were processed via gas atomization and densified by hot pressing (HP). The effects of Sc addition on the microstructure, mechanical properties, fractography, and thermo-physical properties of these alloys have been investigated and discussed.

2 Experimental procedure

2.1 Materials preparation

Al–50Si and Al–50Si–0.3Sc (wt%) alloys power were prepared by gas atomization in an N_2 atmosphere. A mechanical sieve was used to obtain powder with a particle size of more than 200 mesh. These two powders were cold compacted by using a steel mold for a holding time of 2 min. After the cold pressing, some small ingots with micropores can be obtained.

The compacts were subjected to hot pressing at 565 °C for 120 min. The maximum holding pressure was 45 MPa. The heating rate from room temperature was 15 °C/min. The hot press temperature was showed by a thermocouple preset in the graphite mold. The sintering pressure in the furnace was released when the sample temperature dropped to 200 °C, and then the temperature is lowered to room temperature. After hot pressing, an alloy ingot having a diameter of 50 mm and a thickness of 10 mm was obtained. The elemental chemical compositions of the alloys after hot pressing are analyzed to ensure that it meets the composition design requirements. The contents of each element in the alloy and the result are shown in Table 1.

2.2 Characterization

The hot-pressed alloys were machined to obtain microstructural observation and performance test samples. Three parallel samples were taken for each group of materials for performance testing. After the sample was ground, polished, and etched, the microstructure and Si phase morphology were observed using a scanning electron microscope (SEM). Specimens for observation were etched by the Keller reagent for 30 s. The phase structure of the two Al–Si alloys was analyzed by x-ray diffraction (XRD) at a scanning angle of 25°–85°. The composition, morphology, and distribution of secondary phase were observed using transmission electron microscopy (TEM). Specimens for TEM observation were mechanical polished to 50 μm thickness and then thinned by ion polishing. Elemental analysis was tested using electron microprobe (EMPA).

The tensile strength and three-point bending tests of samples were tested on an electronic universal material testing machine (MTS 850). The tensile specimens at room temperature were made into a dumbbell shape according to the standard, and the size of the flexural specimen was 3 mm × 10 mm × 50 mm. The fractured surfaces of the specimens were observed under scanning electron microscopy and it is necessary to ensure the cleaning of the fracture. The Brinell hardness test of the alloy had a load of 7.35 kN for 30 s. Under the argon atmosphere, the thermal expansion coefficient of the two samples was measured in the range of 50–400 °C. The test sample has a size of 20 mm × 5 mm × 5 mm and is required to be parallel and smooth at both ends. The thermal conductivity of both alloys was performed on cylindrical slice specimens and the size of specimens was Φ10 mm × 3 mm. The density of the alloys was measured using an electronic balance.

3 Results and discussion

3.1 Microstructural characteristics

Figure 1 shows the typical microstructure of the Al–50Si alloys prepared by traditionally ingot metallurgy and gas-atomized followed by hot pressing. The large bar-like primary Si with a size of about 300 μm (Fig. 1a) and the eutectic Si with needle-like morphology (Fig. 1b) exist in the as-cast Al–Si alloy. Additionally, the eutectic Si phase with sharp corners and defects are observed. These characteristics of primary and eutectic Si phase are highly detrimental to the mechanical

Table 1 Chemical composition of the hot-pressed Al–50Si and Al–50Si–0.3Sc alloys (mass%)

Alloy	Si	Sc	Fe	Mn	Others	Al
Al–50Si	50.3	–	0.03	0.02	< 0.1	Bal.
Al–50Si–0.3Sc	50.2	0.28	0.04	0.02	< 0.1	Bal.

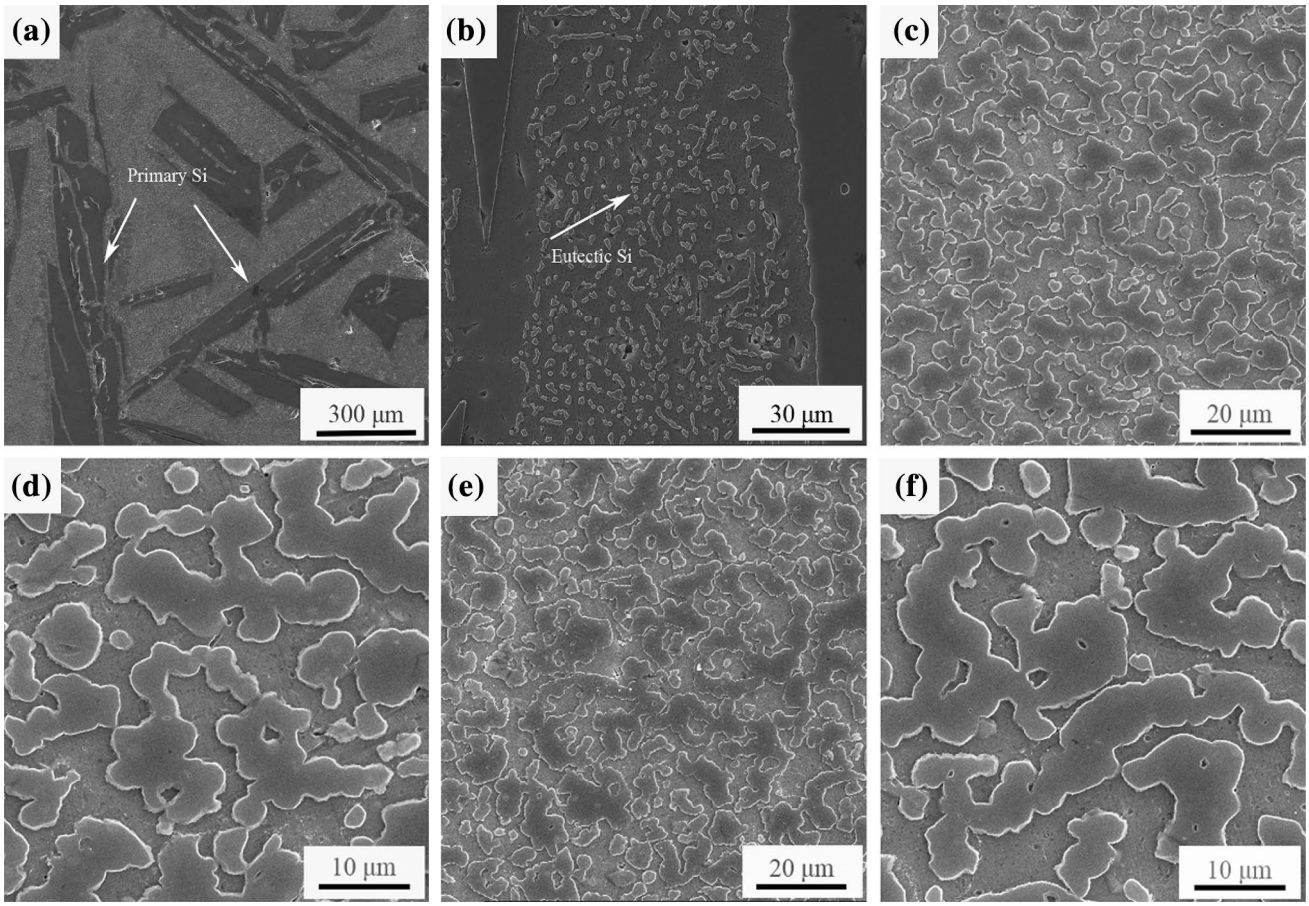

Fig. 1 SEM morphology of the ingot metallurgy Al–50Si alloy with large bar-like primary Si phase and clear defects (**a**, **b**), hot-pressed Al–50Si (**c**, **d**) and Al–50Si–0.3Sc (**e**, **f**) alloys with network Si phase having a smooth surface

properties of Al–Si alloys. Furthermore, the high amount of eutectic Si has a scattering effect on electrons, which reduces the thermal conductivity of the alloy.

When rapid solidification technique is applied, the Si phase exhibits a semi-continuous network structure in the hot-pressed Al–Si alloys. While the surface of Si phase becomes relatively smooth, the size of the Si phase is also refined remarkably, with an average size of 15–20 μm. Compared with the as-cast Al–50Si alloy, this fine and uniformly distributed structure causes a homogeneous distribution of stress in the material, thereby improving the properties of alloys.

However, in comparison with Fig. 1c, d, e, f, the influence of minor alloying with 0.3% Sc did not significantly change the size and morphology of the Si phase. This phenomenon can be attributed to the high sintering temperature and long holding time of hot pressing to obtain a near fully dense microstructure.

During the process of cold pressing, porosity is found in the ingots due to the entrapment of the atomizing gas, and densification by hot pressing is required to eliminate the pores. The measured densities, theoretical densities, and relative densities of the two alloys prepared by hot pressing are illustrated in Table 2. The theoretical density is calculated according to the volume fraction of the two alloys. It is seen that a relative density of 99.7% and 99.8% is obtained in Al–50Si and Al–50Si–0.3Sc alloy, respectively.

Figure 2 shows the XRD patterns of the hot-pressed Al–50Si and Al–50Si–0.3Sc alloys. It is found that only Al and Si phase are detected in the two alloys. This phenomenon is due to the addition of small amount of Sc (0.3 wt%) and the phase containing Sc or other potential intermetallic compounds is too low to be detect by XRD.

Table 2 Measured density and relative density of the hot-pressed Al–50Si and Al–50Si–0.3Sc alloys

Material	Measured density (g/cm^3)	Theoretical density (g/cm^3)	Relative density (%)
Al–50Si	2.497 ± 0.041	2.503	99.7
Al–50Si–0.3Sc	2.498 ± 0.026	2.502	99.8

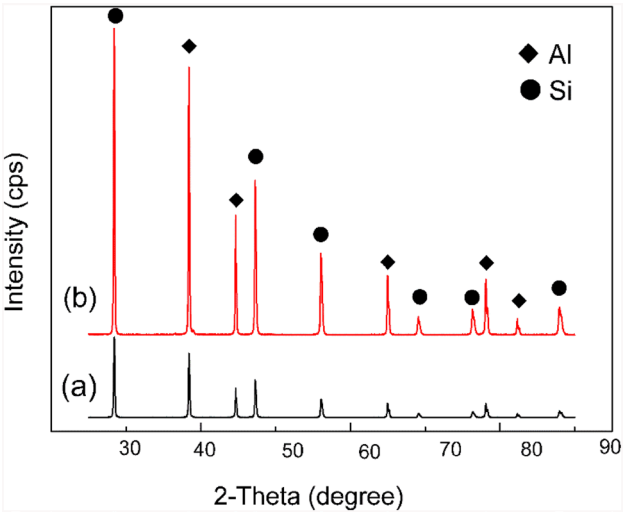

Fig. 2 XRD pattern of the hot-pressed *a* Al–50Si and *b* Al–50Si–0.3Sc alloys

The electron probe surface analysis of the Sc element distribution in the hot-pressed Al–50Si–0.3Sc alloy is presented in Fig. 3. As shown in Fig. 3d, the black and gray phases are the Al matrix and the Si phase, respectively. According to the distribution of Sc elements on EPMA diagram, a small amount of Sc atoms is dissolved into the matrix, but most of them are distributed at the interface between Al matrix and the Si phase.

Figure 4 shows the TEM images of the Al–50Si–0.3Sc alloy. There is an approximately spherical black phase at the interface between the matrix and the Si phase in Fig. 4a. The composition of the black phase in Fig. 4a was determined by energy spectrum analysis. It is obvious that the atomic ratio of the three elements of Al, Si, and Sc is close to 1:2:2 from the analysis results of Fig. 4c. According to the literature about Sc alloying in Al–Si alloys [19], the black phase is the $AlSi_2Sc_2$ phase (V-phase). It has been reported that the addition of more than 0.1 wt% Si to Sc-contained Al alloy can inhibit the formation of Al_3Sc phase which is formed in the Al–Sc binary alloys [17]. The results of Pramod et al. [20] indicated that by introducing Sc to the A356 alloys, the lattice parameter of α-Al phase was increased. This is a piece of clear evidence that Sc has a solid solution strengthening on the Al matrix. Additionally, the strength of Sc-contained alloy may also be enhanced by the formation of nanoscale second phase which hinders the movement of dislocations.

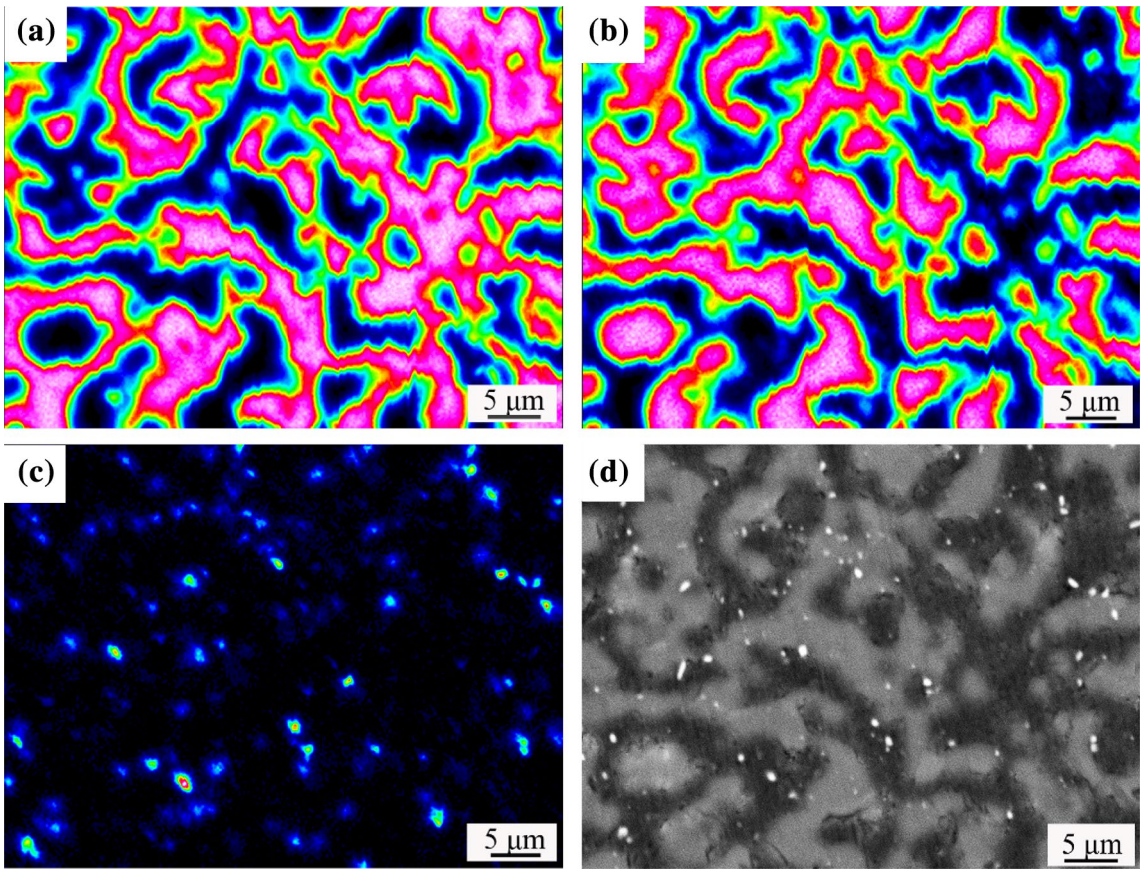

Fig. 3 Elemental maps of the Al–50Si–0.3Sc alloy **a** Al mapping, **b** Si mapping, **c** Sc mapping, **d** backscattered micrograph

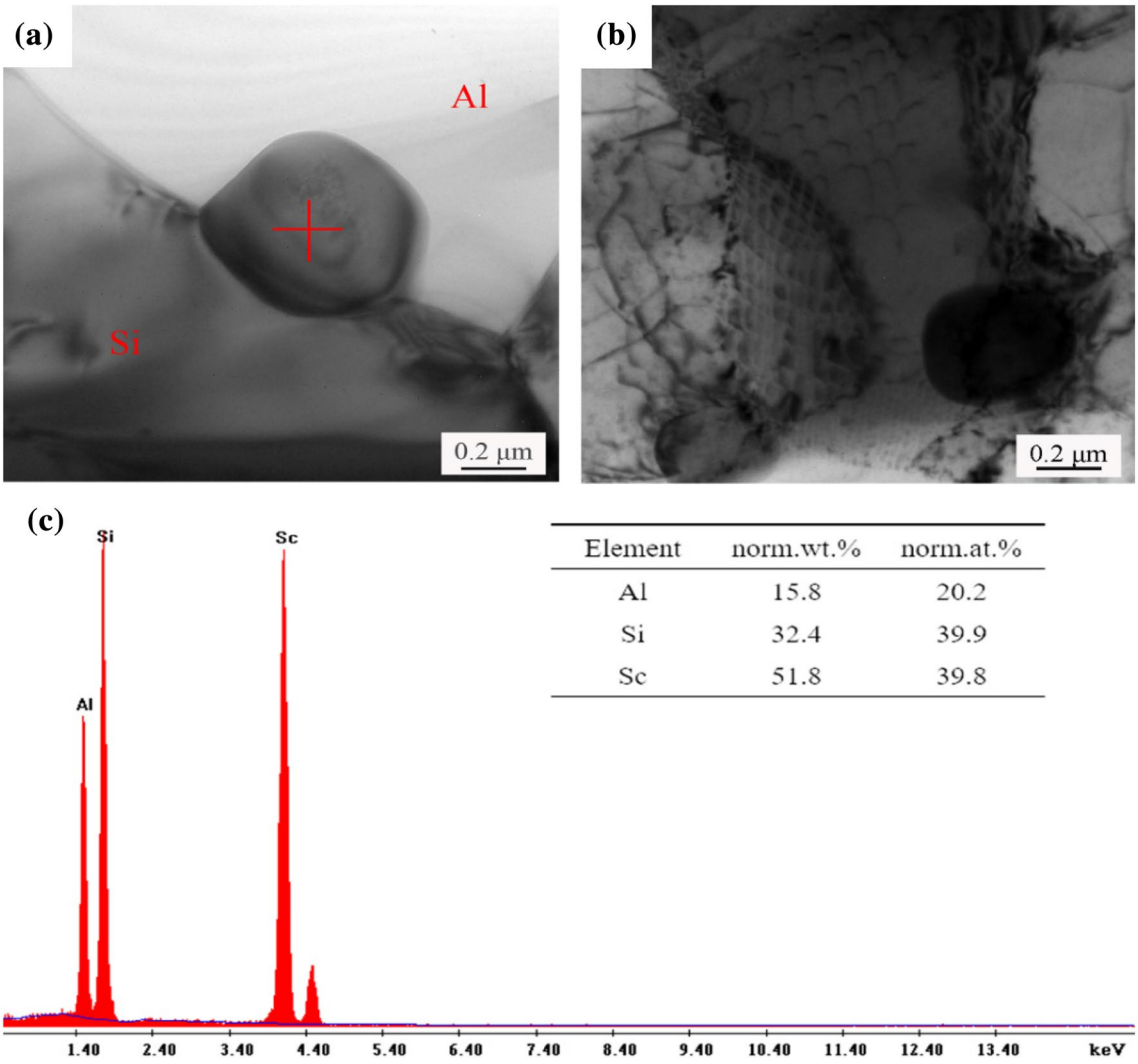

Element	norm.wt.%	norm.at.%
Al	15.8	20.2
Si	32.4	39.9
Sc	51.8	39.8

Fig. 4 TEM micrographs (**a**, **b**) of the Al-50S-0.3Sc alloy and TEM–EDS analysis result (**c**) of the black phase in (**a**)

From the distribution of $AlSi_2Sc_2$ phase, only the phase distributed at the interface can inhibit the diffusion of Si atoms and slow the thermal activation of Si phase. The $AlSi_2Sc_2$ phase distributed in the matrix has little effect on Si phase. This phenomenon is similar to the effect of modifiers on primary Si in the as-cast Al–Si alloys [21]. However, the high hot press temperature and long holding time lead to the negligible influence of the $AlSi_2Sc_2$ phase located at the interface on the coarsening of Si phase.

3.2 Thermo-physical properties

Thermal conductivity of the hot-pressed Al–50Si alloys is shown in Fig. 5. It can be seen that the thermal conductivity of both alloys decreases with the increasing temperature. The addition of minor Sc element causes the thermal conductivity to decrease from 146 to 143 W/(m·K) at room temperature.

In metal matrix composites, the matrix metal or alloy transfers heat primarily through free electrons, and the reinforcement is generally non-metallic, primarily transferring heat through phonons. The presence of the second phase has a certain scattering effect on the movement of the free electrons, hindering the conductance of the heat conduction [22]. For the Al–50Si alloys, the thermal conductivity mainly depends on the thermal conductivity of each component, the volume fraction, size and distribution of the reinforcement [23]. These two Al–Si alloys have almost no difference in the Si content and microstructure. However, the movement of free electrons is hindered by the scattering of the fine $AlSi_2Sc_2$ phase, which reduces the thermal conductivity of the Al matrix. Therefore, the thermal conductivity of Al–50Si–0.3Sc alloy is reduced by approximately 2.1%.

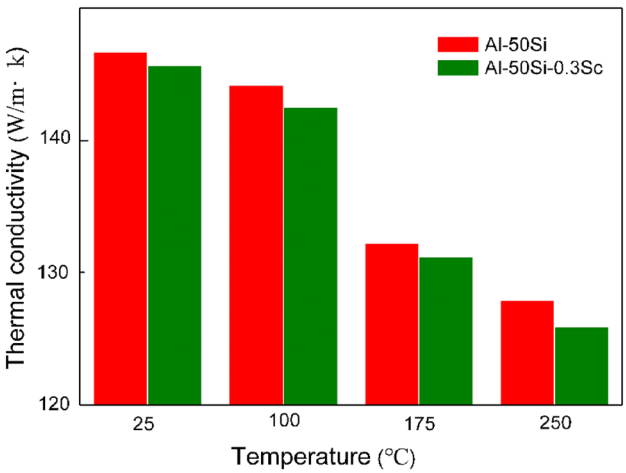

Fig. 5 Thermal conductivity of the hot-pressed Al–50Si and Al–50Si–0.3Sc alloys at different temperatures

Figure 6 shows the relationship between the CTE and temperature of the Al–50Si and Al–50Si–0.3Sc alloys. The results show that the CTE of the two alloys has a consistent trend with temperature. However, the CTE of the Sc-containing alloy is a little lower than that of the Sc-free alloy at all measured temperatures.

The thermal expansion coefficient of the Si reinforcement (4.2×10^{-6}/K) is much lower than that of the Al matrix (about 23.6×10^{-6}/K). At the lower temperatures, the Al matrix does not undergo obvious plastic deformation. The thermal expansion is a combination of the Al matrix and the Si particles, and the CTE of the Al–50Si alloys increases with the increasing temperature. However, as the temperature continues to rise, the interfacial thermal stress in the alloy increases gradually and the yield strength of the Al matrix decreases at the same time. At the elevated temperature, when the thermal stress exceeds the yield strength, the Al matrix may be plastically deformed [24, 25]. The thermal expansion of the alloy is mainly attributed to the Al matrix, while the plastic deformation of the Si phase and the matrix may offset the expansion of the partial Al matrix. Additionally, Jia et al. [8] found that the rapid solidification technique will obtain a higher cooling rate, and some of the Al atoms will dissolve into the Si phase, which will reduce the CTE to some extent. The V-phase distributed at the interface and the matrix creates a lot of new interfaces that effectively constrain the expansion of the matrix.

3.3 Mechanical performance

The tensile curves of the hot-pressed alloys are depicted in Fig. 7. It can be seen that both the alloys have the same stress–strain response, and the elongation is low without obvious plastic deformation characteristics. The mechanical properties of the two alloys are listed in Table 3. Compared with the Sc-free alloy, the tensile strength of Al–50Si–0.3Sc alloy increases from 183 to 225.2 MPa, an increment of approximately 16.2%. Additionally, the Al–50Si–0.3Sc alloy reaches a bending strength of 331 MPa, which is 8.9% higher than that of the Al–50Si alloy. The tensile and flexural strength of the Al–50Si alloy with alloying elements are mainly depending on two aspects: one is the size of the Si phase; the other is the strengthening effect of the alloying elements on the Al matrix. From the previous analysis, it is known that the addition of 0.3% Sc in this experiment does not change the size and morphology of the Si phase. However, the precipitation of fine and evenly distributed $AlSi_2Sc_2$ phase strengthens the Al matrix, thereby increasing the tensile strength and bending strength of the alloy.

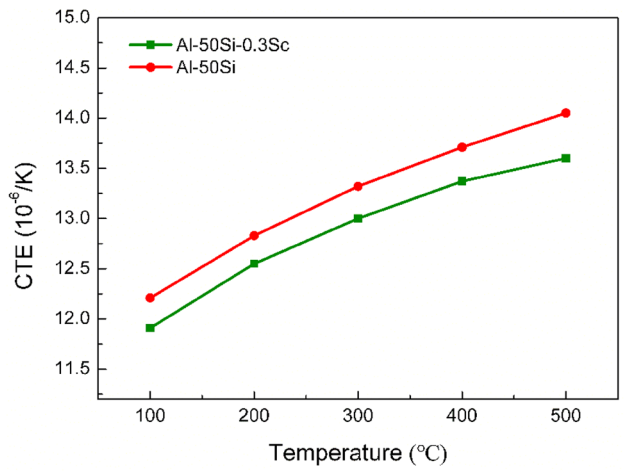

Fig. 6 Coefficient of thermal expansion of the hot-pressed Al–50Si and Al–50Si–0.3Sc alloys as a function of temperature (10^{-6}/K)

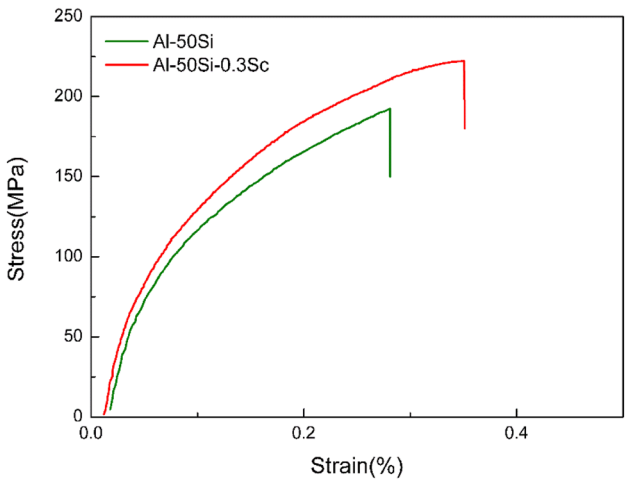

Fig. 7 Schematic stress–strain behavior of the hot-pressed Al–50Si and Al–50Si–0.3Sc alloys at room temperature

Table 3 Mechanical properties of the hot-pressed Al–50Si and Al–50Si–0.3Sc alloys

Specimen	Tensile strength (MPa)	Bending strength (MPa)	Micro-hardness (HBS)
Al–50Si	183	304	142
Al–50Si–0.3Sc	225	331	163

Additionally, Nadimpalli et al. [26] studied the spray-formed Al–*x*Si–0.8Sc ($x = 13$, 16, 19 and 22 wt%) alloys and found that the morphology and size of the same content of the reinforcement are not greatly different under the same molding process, and the presence of the $AlSi_2Sc_2$ phase can significantly improve the strength of matrix.

The tensile fracture morphology of the Al–50Si alloys is presented in Fig. 8. The fracture surface of all the samples is flat, perpendicular to the tensile direction, and having no obvious plastic deformation. This is a typical brittle fracture feature which is consistent with the tensile stress–strain results. The fracture morphology of the Al–Si alloy is almost the same as that of the sample in which the Sc element is added. From the morphology of the low-magnification image, it can be found that the crack source of the material is initiated on the surface of the tensile specimen, and then gradually expands to the inside. This phenomenon indicates that the internal structure of the material is free of defects such as inclusions. Additionally, the surface at the source of the fracture is relatively flat compared to the other places. In high-magnification images, most of the cracks develop from the Si particles and extend from one particle to the other through the matrix [27]. Part of the cracks appear at the interface junction between the Si phase and the Al matrix because of the stress concentration and the presence of brittle $AlSi_2Sc_2$ phase at the interface. The fracture mode of the Al matrix is a ductile fracture, while the Si phase is cleavage fracture. At the same time, since Si has a certain solid solubility in Al, it has good wettability, and no interfacial reaction occurs during the molding process, so it has a strong interfacial bonding. No peeling of the interface is observed at the fracture after stretching.

4 Conclusion

In the present study, the Al–50Si and Al–50Si–0.3Sc alloys were prepared by rapid solidification technology following hot press sintering. The microstructure and properties of the Al–Si alloys with and without adding Sc element were analyzed. The following conclusions can be summarized:

(1) The uniform and dense Al–Si alloy can be obtained by hot pressing, and the Si phase exhibits a three-dimensional network structure with an average size of 15–20 μm. The Si phase in the Al–Si alloy does not change significantly with the addition of a small amount of Sc (0.3%). The nanoscale spherical $AlSi_2Sc_2$ phase is mainly distributed at the interface between the Si phase and Al matrix.

(2) Compared with the Al–50Si alloy, the tensile strength, flexural strength, and hardness of the Al–50Si–0.3Sc alloy increase by 16.2%, 8.9%, and 14.7%, respectively, due to the strengthening of the matrix by the micro-dispersed $AlSi_2Sc_2$ phase. Although the addition of the Sc element causes a slight decrease in thermal expansion coefficient and thermal conductivity, it can still be regarded as a qualified electronic packaging material.

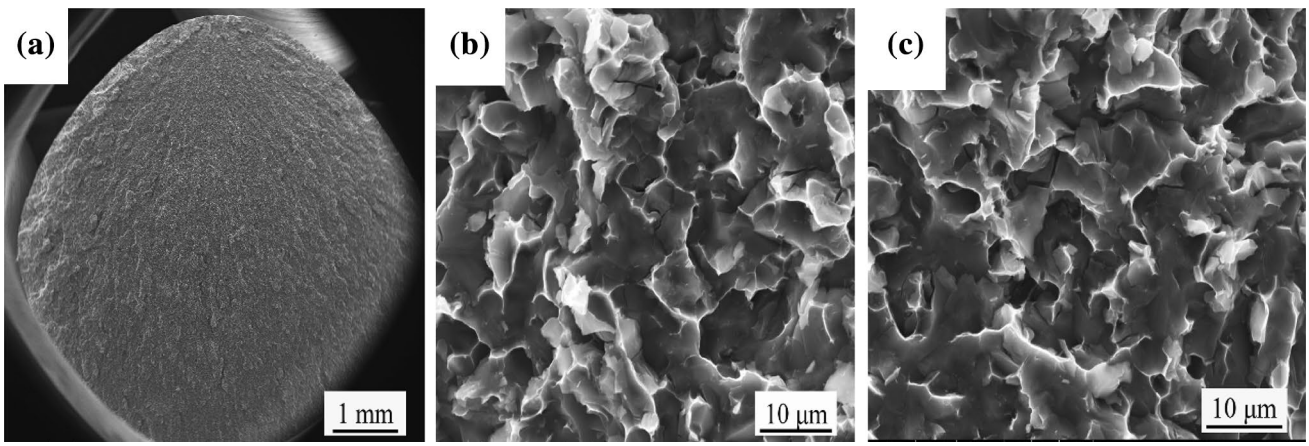

Fig. 8 Low-magnified (**a**) and magnified (**b**) micrograph of the crack source of the Al–50Si alloy, **c** typical magnified fractography of the Al–50Si–0.3Sc alloy

Acknowledgement The authors are grateful for the financial support provided by the National Nature Science Foundation of China (51804349), the China Postdoctoral Science Foundation (2018M632986), the Nature Science Foundation of Hunan Province (2019JJ50766), and the Postdoctoral Science Foundation of Central South University and the Science and Technology Program of Hunan, China (2017GK2261).

References

1. Y.B. Tang, H.T. Cong, R. Zhong, H.M. Cheng, Carbon **42**(15), 3260–3262 (2004)
2. C. Cui, A. Schulz, J. Epp, H.W. Zoch, J. Mater. Sci. **45**(10), 2798–2807 (2010)
3. W.K. Kang, F. Yilmaz, H.S. Kim, J.M. Koo, S.J. Hong, J. Alloys Compd. **536**(S1), S45–S49 (2012)
4. F. Wang, B.Q. Xiong, Y.A. Zhang, B.H. Zhu, H.W. Liu, Y.G. Wei, Mater. Charact. **59**(10), 1455–1457 (2008)
5. S.C. Hogg, A. Lambourne, A. Ogilvy, P.S. Grant, Scr. Mater. **55**(1), 111–114 (2006)
6. Y.D. Jia, P. Ma, K.G. Prashanth, G. Wang, J. Yi, S. Scudino, F.Y. Cao, J.F. Sun, J. Eckert, J. Alloys Compd. **699**, 548–553 (2017)
7. Q.L. Li, T.D. Xia, Y.F. Lan, W.J. Zhao, L. Fan, P.F. Li, J. Alloys Compd. **577**, 232–236 (2013)
8. Y.D. Jia, F.Y. Cao, S. Scudino, P. Ma, H.C. Li, L. Yu, J. Eckert, J.F. Sun, Mater. Des. **57**, 585–591 (2014)
9. Z.J. Wei, P. Ma, H.W. Wang, C.M. Zou, S. Scudino, K.K. Song, K.G. Prashanth, W. Jiang, J. Eckert, Mater. Des. **65**, 387–394 (2015)
10. S. Furuta, M. Kobayashi, K. Uesugi, A. Takeuchi, T. Aoba, H. Miurab, Mater. Charact. **130**, 237–242 (2017)
11. Q.L. Li, T.D. Xia, Y.F. Lan, W.J. Zhao, L. Fan, P.F. Li, J. Alloys Compd. **562**, 25–32 (2013)
12. W.X. Shi, B. Gao, G.F. Tu, G.F. Tu, S.W. Li, J. Alloys Compd. **508**, 480–485 (2010)
13. Q.L. Li, B.Q. Li, J.B. Li, C.H. Zhang, Mater. Sci. Forum **893**, 202–206 (2017)
14. S.C. Hogg, H.V. Atkinson, Metall. Mater. Trans. A **36**(1), 149–159 (2005)
15. W. Zhang, Y. Liu, J. Yang, J.Z. Dang, H. Xu, Z.M. Du, Mater. Charact. **66**, 104–110 (2012)
16. M. Kim, Met. Mater. Int. **13**(2), 103–107 (2007)
17. J. Røyset, N. Ryum, Int. Mater. Rev. **50**(1), 19–44 (2005)
18. F.G. Leonardo, J.E. Spinelli, A.A. Bogno, M. Gallerneault, H. Heneih, J. Alloys. Compd. **785**, 1077–1085 (2019)
19. N. Raghukiran, R. Kumar, Mater. Sci. Eng., A **657**, 123–135 (2016)
20. S.L. Pramod, A.K.P. Rao, B.S. Murty, S.R. Bakshi, Mater. Sci. Eng. A. **674**, 438–450 (2016)
21. J.Y. Chang, G.H. Kim, I.G. Moon, C.S. Choi, Scr. Mater. **39**(3), 307–314 (1998)
22. L.C. Davis, B.E. Artz, J. Appl. Phys. **77**, 4954–4960 (1995)
23. Z.Y. Cai, C. Zhang, R.C. Wang, C.Q. Peng, K. Qiu, Y. Feng, Mater. Des. **87**, 996–1002 (2015)
24. S. Elomari, M.D. Skibo, A. Sundarrajan, H. Richards, Compos. Sci. Technol. **58**, 369–376 (1998)
25. T.A. Hahn, R.W. Armstrong, Int. J. Thermophys. **9**, 179–193 (1988)
26. N. Raghukiran, R. Kumar, Mater. Sci. Eng. A **641**, 138–147 (2015)
27. Z.Y. Cai, C. Zhang, R.C. Wang, C.Q. Peng, X. Wu, H.P. Li, Mater. Sci. Eng. A **730**, 57–65 (2018)